Cell to network computational model of the epileptic human hippocampus suggests specific roles of network and channel dysfunctions in the ictal and interictal oscillations

Amélie Aussel, Radu Ranta, Olivier Aron, Sophie Colnat-Coulbois, Louise Tyvaert, Louis Maillard, Laure Buhry

Noname manuscript No.
(will be inserted by the editor)

Cell to network computational model of the epileptic human hippocampus suggests specific roles of network and channel dysfunctions in the ictal and interictal oscillations

Amélie Aussel · Radu Ranta · Olivier Aron · Sophie Colnat-Coulbois · Louise Tyvaert · Louis Maillard · Laure Buhry

the date of receipt and acceptance should be inserted later

Abstract The mechanisms underlying the generation of hippocampal epileptic seizures and interictal events and their interactions with the sleep-wake cycle are not yet fully understood. Indeed, medial temporal lobe epilepsy is associated with hippocampal abnormalities both at the neuronal (channelopathies, impaired potassium and chloride dynamics) and network level (neuronal and axonal loss, mossy fiber sprouting), with more frequent seizures during wakefulness compared with slow-wave sleep. In this article, starting from our previous computational modeling work of the hippocampal formation based on realistic topology and synaptic connectivity, we study the role of micro- and mesoscale pathological conditions of the epileptic hippocampus in the generation and maintenance of seizure-like theta and interictal oscillations. We show, through the simulations of hippocampal activity during slow-wave sleep and wakefulness that: (i) both mossy fiber sprouting and sclerosis account for seizure-like theta activity, (ii) but they have antagonist effects (seizure-like activity occurrence increases with sprouting but decreases with sclerosis), (iii) though impaired potassium and chloride dynamics have little influence on the generation of seizure-like activity, they do play a role on the generation of interictal patterns, and (iv) seizure-like activity and fast ripples are more likely to occur during wakefulness and interictal spikes during sleep.

Keywords hippocampus, computational modeling, epilepsy, sleep-wake cycle, realistic anatomy, pathological connectivity

A. Aussel E-mail: amelie.aussel@inria.fr *Present address: INRIA Bordeaux Sud-Ouest, Talence, France*
A. Aussel · L. Buhry
Laboratoire Lorrain de Recherche en Informatique et ses applications (LORIA UMR 7503, University of Lorraine-INRIA-CNRS, F-54506)

A. Aussel · L. O. Aron · S. Colnat-Coulbois · L. Tyvaert · L.Maillard · R. Ranta
Centre de Recherche en Automatique de Nancy (CRAN-CNRS UMR 7039 University of Lorraine, FRANCE)

O. Aron · S. Colnat-Coulbois · L. Tyvaert · L.Maillard
Department of Neurology, CHU de Nancy, Nancy, FRANCE.

1 Introduction

The hippocampus can exhibit oscillatory rhythms in a wide range of frequencies, depending on the cognitive task to perform, the vigilance state, the possible pathological state, etc. Altered hippocampal rhythms are involved in medial temporal lobe epilepsy, the most frequent form of focal epilepsy, often pharmacoresistant and affecting about 0.6 person per 1000 people [Asadi-Pooya et al., 2017]. Beside hippocampal seizures (complex phenomena typically consisting in episodes of abnormal, excessive and/or hypersynchronous neural activity, as defined in [Fisher et al., 2014] or [Jiruska et al., 2013]), the epileptic hippocampus also produces frequent interictal epileptic abnormal rhythms which have been shown to be associated with cognitive impairments of episodic memory ([Krauss et al., 1997]), memory maintenance and retrieval ([Kleen et al., 2013]), and memory consolidation ([Gelinas et al., 2016]).

Some computational models have been previously developed to reproduce epileptic seizures (see the review from [Stefanescu et al., 2012]) or interictal spikes (brief peaks of synchronous activity, see for example [Demont-Guignard et al., 2009]), but these models cannot fully explain the correlations between neuropathological conditions of the hippocampus, physiological processes such as the sleep-wake cycle, and the resulting oscillations (note still that a broader view can be found in [Jiruska et al., 2014]). Indeed, computational models have typically studied epileptic phenomena at a single scale ([Wendling et al., 2012]). They usually focus either, on one hand, on microscopic mechanisms with rather detailed neuron models, but only small hippocampal substructures [Demont-Guignard et al., 2009, Ratnadurai Giridharan et al., 2014], which do not allow to take into account the specificity of the hippocampal anatomy and connectivity responsible for the richness of the produced rhythms; or, on the second hand, on macroscopic features that grant importance to connectivity patterns and excitation/inhibition balance, while the implication of intracellular dynamics, which also affects rhythm genesis, remains unclear.

One can cite, among computational studies focusing on cellular pathologies, the work of [Cressman et al., 2009] on the role of potassium and sodium dynamics, or [Dyhrfjeld-Johnsen, 2008] on the role of hyperpolarization activated current (other computational models of the epileptic dentate gyrus can be found in [Tejada and Roque, 2014]). At the network level, [Wendling et al., 2002] model the synaptic coupling between neuronal populations and take into account different types of populations of inhibitory and excitatory neurons, [Netoff, 2004] reproduce the topology of synaptic connections, [Morgan and Soltesz, 2008] study the role of sclerosis and mossy fiber sprouting. Some more recent works focus on epileptic cortical tissue but have interesting conclusions on epileptic networks and their dynamics in general. One can cite [Liou et al., 2020] which developed a 2-D model studying seizure onset and propagation in relation with synaptic plasticity and noise, and [Rich et al., 2022] which tackles the link between reduced network heterogeneity and ictogenic dynamics. However, all these works at the network level do not explicitly address the role of intracellular mechanisms. Overall, and as is also pointed by [van den Heuvel et al., 2019], this highlights the need for a multi-scale model comprising the joint effects of both network and microscopic properties.

In this context, the main objective of this article is to provide better understanding of pathological hippocampal oscillations: epileptic seizures, interictal spikes and fast ripples. We do so by developing a multi-scale computational model of the hippocampus regrouping many mechanisms previously described in separate works, and analyzing its oscillatory activity as we vary different parameters representing either structural or functional properties of the network, associated with pathological modifications typically observed in epilepsy.

More precisely, we extend a healthy hippocampus model of the sleep-wake cycle we previously presented in [Aussel et al., 2018] so as to include four typical pathological modifications of the hippocampus seen in medial temporal lobe epilepsies. In particular, we focus on hippocampal sclerosis ([Blümcke et al., 2013]), mossy fiber sprouting ([Noebels et al., 2012]), impaired potassium dynamics ([Lerche et al., 2012], [Coulter and Steinhauser, 2015]), and impaired chloride dynamics in pyramidal neurons (and its influence on inhibition, [Huberfeld et al., 2007]). These modifications involve both network connectivity and single neuron dynamics. The model also includes a simulation of the Local Field Potential (LFP) generated by the neurons, so as to be comparable with clinical recordings. Typically, we aim to reproduce morphologies and rhythms in specific frequency bands characteristic for ictal or interictal events and extensively explore the ranges of parameters that give rise to them, rather than fitting one individual's precise recordings.

In the present work, we first analyze our pathological hippocampal network's behavior under stereotypical inputs, and study how the four parameters representing hippocampal sclerosis, mossy fiber sprouting, impaired potassium dynamics and impaired chloride dynamics can induce saturation or modify neural oscillatory fre-

quency. We also investigate whether the specific functional connectivity of wakefulness induced by cholinergic modulation could make this state more vulnerable to epilepsy-associated damage.

We then move to a more realistic simulation and apply signals derived from intracerebral recordings of individuals with epilepsy as inputs to the network in order to compare the LFP output of our model to real recordings. The aim is to assess which parameter settings enable the reproduction, at the LFP output of the model, of some characteristics of a clinically recorded hippocampal seizure in the theta frequency band, as well as of different interictal patterns (interictal spikes and fast ripples). More precisely, we show that mossy fiber sprouting and hippocampal sclerosis determine the appearance of seizure-like theta activity in the model (the former parameter facilitates it while the latter hinders it), whereas impaired potassium and chloride dynamics mostly affect the number of interictal events.

After presenting the detailed results of these different simulations, we focus our discussion on the role and the balance of the modeled phenomena in epilepsy. We examine how the network related pathologies (mossy fiber sprouting and sclerosis) and the cellular mechanisms (potassium and chloride dynamics) can affect seizure-like theta episodes and interictal events generation, in both sleep and wakefulness states. We finally discuss the implications of our study of hippocampal rhythms on cognitive impairments, essentially memory deficits, usually associated with hippocampal epilepsy.

2 Materials and Methods

In the following subsections, we will briefly present the main features of our model of the healthy hippocampus (developed in details in [Aussel et al., 2018] and whose parameters were explored in [Aussel et al., 2021]), before showing how it was modified to account for epileptic abnormalities. We will then explain thoroughly how we simulated and analyzed the behavior of this epileptic model.

2.1 Computational modeling of healthy hippocampal oscillations

The model proposed in this paper is directly inspired from our previous work ([Aussel et al., 2018]). We recall that this model covers multiple scales, from channel level mechanisms (Hodgkin-Huxley formalism, used to model classical K and Na channels, but also Calcium-Activated Nonselective cation channel - CAN) to realistic anatomy and modulated connectivity (intra and inter structures connection probabilities and gains on synaptic conductances). The model includes more than thirty thousand neurons to represent the four main regions of the hippocampal formation: the Dentate Gyrus (DG), CA3, CA1, and the entorhinal cortex (EC). The number of neurons in each region and the proportion of excitatory and inhibitory cells were chosen in accordance with the literature ([Jinno and Kosaka, 2010], [West and Gundersen, 1990], [Patton and McNaughton, 1995], see [Aussel et al., 2018] for a detailed explanation). The neuron models we use are taken from [Giovannini et al., 2017], which themselves trace back to the work on hippocampal neurons by [Jochems and Yoshida, 2015] (and explains the role of the CAN channel in the persistent firing involved in memory). The model is driven by a set of parameters (gains, maximum probabilities, input characteristics), themselves with biological significance. The complete structure is given Figure 1. In our previous paper, we have proposed a set of parameters (in blue in Figure 1-B and C) and mechanisms able to explain sleep-wake variations of the oscillatory patterns (sharp-wave ripples and theta-gamma) and the transitions between them. For details, see [Aussel et al., 2018] and [Aussel et al., 2021].

2.2 Model changes to account for epilepsy

Among the different changes that can occur in an epileptic hippocampus, we chose to focus on four of the most frequent in particular: hippocampal sclerosis, mossy fiber sprouting, increased excitability and impaired inhibition of excitatory neurons. For simplicity reasons, these changes have been targeted exclusively at excitatory cells (their number, synaptic connectivity, potassium and chloride dynamics), but have been chosen so as to provide an overview of the effect of both cell and network pathologies on hippocampal dynamics. Parameters linked to epilepsy in the model appear in red in Figure 1.

Hippocampal sclerosis was modeled by reducing the number of excitatory neurons in each subregion of the model as a fraction scl of the maximum pyramidal cell and granule cell reduction observed in type 1 hippocampal sclerosis (see [Blümcke et al., 2013]). More precisely, the number of excitatory neurons was set to :

- $10000 \cdot (1 - 0.75scl)$ in the entorhinal cortex
- $10000 \cdot (1 - 0.6scl)$ in the dentate gyrus
- $1000 \cdot (1 - 0.8scl)$ in CA3
- $10000 \cdot (1 - 0.8scl)$ in CA1

with scl varying between 0 (no sclerosis) and 1 (high sclerosis). With $scl = 0$, the number of excitatory neu-

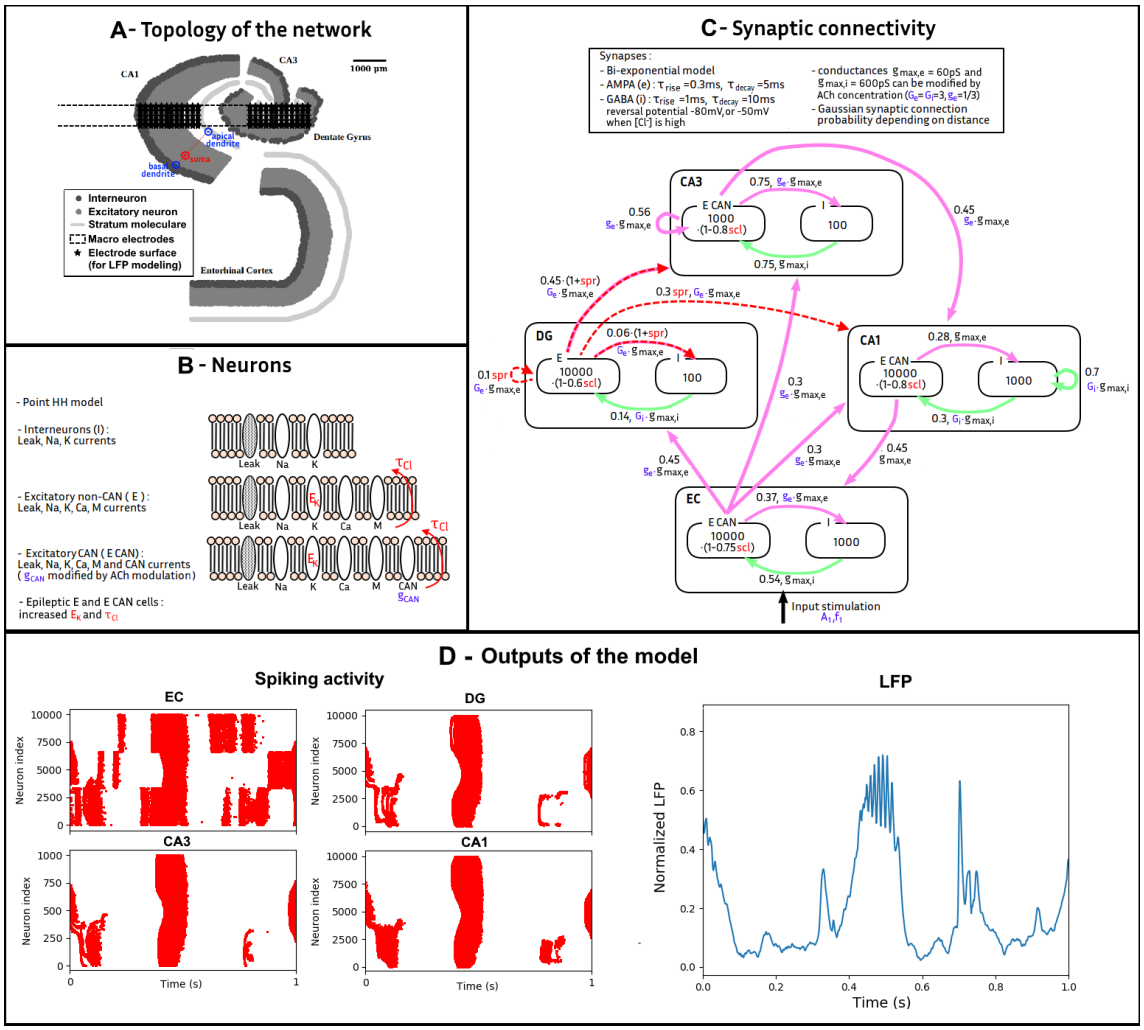

Fig. 1 A- Topology of the entorhinal cortex and the hippocampus used in the model, along with the two simulated electrode contacts, adapted from [Aussel et al., 2018]. B- Membrane channels of the neuron models used in the network. C- Synaptic connectivity of our model of the hippocampal formation. The number of neurons of each type in each region is shown inside black boxes. Purple arrows represent AMPA synaptic interactions, and green arrows represent GABA synaptic interactions, with next to them the corresponding connection probability and the maximum synaptic conductance. The black arrow represent input stimulation given to the EC neural populations. In panels B and C, the parameters linked to the sleep-wake cycle appear in blue and the parameters linked to epilepsy appear in red. D- Outputs of the model. Left : Raster plots of the excitatory cells activity during 1 second of simulation. Right : Local field potential generated by the network during the same simulation.

rons in all regions is the same as in our healthy hippocampus model. The number of inhibitory neurons on the other hand was left unchanged for several main reasons: first, they are not included in the typical definition of hippocampal sclerosis ([Blümcke et al., 2013]); second, no inhibitory loss was reported in some studies (see for example [Babb et al., 1989]) or, as proposed in other studies (see [Fritschy et al., 1999]), the loss could be compensated by an increased number of GABA-A receptors in remaining cells (nevertheless, we have also simulated the same proportion of neuronal loss on inhibitory cells as on excitatory cells in our model and it did not significantly impact our results (see Figure S1 in appendix).

Mossy fiber sprouting (see [Noebels et al., 2012]) was represented by including recurrent excitatory connections in the dentate gyrus as well as increasing the number of connections from excitatory to inhibitory neurons in this region, and to CA3 and CA1 neurons (see [Bausch and McNamara, 2000] for a study on hippocampal slice cultures), though reciprocal connections from CA3 and CA1 to the DG have not been included. A parameter *spr* varying between 0 (no sprouting) to 1 (high sprouting) was defined to modify the maximum synaptic connection probabilities to:

– $0.1 \cdot spr$ from excitatory to excitatory neurons, so that each excitatory neuron makes in average 300 synapses with $spr = 1$, in accordance with the max-

imum 500 new synapses reported in a pilocarpine epilepsy model in [Buckmaster et al., 2002]
- $0.06 \cdot (1+spr)$ from excitatory to inhibitory neurons, so that each excitatory neuron forms about 1% of its new synapses with inhibitory interneurons.

It should be noted that the additional synapses in the sprouted model obey the same equations as the healthy synapses, and that they too have a higher probability of being drawn between spatially close neurons than between spatially distant neurons.

Regarding the increased excitability of pyramidal cells, we chose to change the equilibrium potential for potassium E_K. Though this parameter by itself is agnostic of the malfunction causing the increased excitability, it could represent for example a channelopathy ([Lerche et al., 2012]). A healthy hippocampus is characterized by $E_K = -100mV$, and this value is increased to $-90mV$ or $-80mV$ to represent epilepsy. As the role of this parameter is to mimic increased excitability in pyramidal cells, this change in E_K was not implemented in interneurons.

Finally, different mechanisms can alter synaptic inhibition in medial temporal lobe epilepsy. The one we focus on here is the accumulation of chloride ions inside pyramidal cells changing the reversal potential of GABA synapses (see [Huberfeld et al., 2007] or [Auer et al., 2020]).

We propose to model chloride ion concentration in each excitatory neuron as a simple first order process:

$$\frac{d[Cl^-]}{dt} = -\frac{[Cl^-]}{\tau_{Cl}} \tag{1}$$

with τ_{Cl} the decay rate of $[Cl^-]$ (similarly to what has been done in different papers such as [O'Leary et al., 2013] on calcium concentration). Whenever the excitatory neuron emits an action potential, the concentration $[Cl^-]$ is then increased by a fixed amount (set here to 0.2). A healthy hippocampus is characterized by a fast τ_{Cl} decay rate of $100ms$; we increased this value up to $0.5s$ or $1s$ to represent the abnormal accumulation of intracellular chloride in epilepsy.

The expression of the resting potential E_I of the inhibitory synaptic current received by the neuron is then modified to :

$$E_I = \begin{cases} -80mV \text{ if } [Cl^-] \leq 0.5 \\ -50mV \text{ otherwise.} \end{cases} \tag{2}$$

i.e., when the concentration of chloride ions inside a neuron gets too high, the reversal potential of the inhibitory synapses received by the neurons is increased to $E_I = -50$ mV (as suggested in the experimental work from [Pathak et al., 2007]), which is above the resting potential of the neuron, and the synapses become excitatory. This model has voluntarily been kept relatively simple as there is to the best of our knowledge no modeling literature on this topic as of today, and [Pathak et al., 2007] suggests that GABA reversal potential can reach a plateau of around -50 mV after only a few spikes. The numerical values involved in the model (the threshold of $[Cl^-]$ above which the synapse gets excitatory, the decay rate of $[Cl^-]$, and the increase of $[Cl^-]$ for each spike) have been chosen empirically after simulation with different values so that inhibitory synapses resting potentials are scarcely modified in a simulation with parameters representing a healthy hippocampus. The alteration of synaptic inhibition is restricted to excitatory neurons in our model, as one of the main mechanisms inducing this pathology, an anomaly in KCC2 transporter expression, has been mostly reported in pyramidal and granule cells of the hippocampus (see [Auer et al., 2020], or [Chamma et al., 2012] for a more general overview on KCC2).

To summarize, our study introduces 4 new pathological parameters in our hippocampal model, scl, spr, E_K and τ_{Cl}, representing respectively hippocampal sclerosis, mossy fiber sprouting, pyramidal cell hyperexcitability and impaired inhibition. These parameters are to be studied in relation with the vigilance state, which can be set to either slow-wave sleep or wakefulness, according to the methodology described in our previous works [Aussel et al., 2018] and [Aussel et al., 2021], and recalled in Table 1.

Parameter	Slow-wave sleep	Wakefulness
G_e	1	3
g_e	1	1/3
G_i	1	3
g_{CAN}	$0.5\mu S/cm^2$	$25\mu S/cm^2$

Table 1 Choice of network parameters for the sleep and wakefulness state

2.3 Output of the hippocampal model: LFP simulation

Our goal is to construct a full model, able to compare with real electrophysiological signals recorded in individuals with epilepsy. But the model described in the previous section is constructed using point neurons, and point neurons cannot generate extracellular potentials, as they do not respect current conservation laws. A minimal neuron model able to generate LFP has to be dipolar ([Pettersen et al., 2012]). As the LFP is thought to

be mainly due to synaptic currents, the neural dipoles are supposed to form between the dendritic and somatic compartments of the neurons.

For each excitatory neuron, its projection on the stratum moleculare was thus computed as an estimation of the position of its apical dendrites (Figure 1-A), and its projection on the stratum oriens as an estimation of the position of its basal dendrites. The synaptic compartments of the neural elementary dipole was set to the basal or apical dendrites depending on the synapse type, following existing literature (see for example [Andersen et al., 2007]). This is slightly different from our previous model [Aussel et al., 2018] where all synapses locations were assigned to the apical dendrite of target neurons. As interneurons contributions to the LFP are very small [Mazzoni et al., 2015], their microscopic geometry and thus the LFP they generate were neglected (point neurons).

The analyzed output is the extracellular potential generated by the network, at a macroscopic scale (an example is shown on Figure 1-D, and an animation is also provided as Supplementary Material).

The modelling of the LFP follows the approach proposed in [Mazzoni et al., 2015]. More precisely, the potential in every point in space was approximated by a weighted sum of the synaptic currents (both excitatory and inhibitory) arriving at each pyramidal neuron (the influence of the synaptic currents arriving onto interneurons was neglected). Considering the neurons as dipoles (with orientation and amplitude given by the above described projections of the soma), the contribution U of a neuron of length L to the extracellular potential at any point in space, at a distance r and an angle θ from the midpoint of the neuron, writes as:

$$U = \frac{L\,cos\,\theta}{4\pi\sigma r^2}\,(I_{syn_E} + I_{syn_I}) \tag{3}$$

where $\sigma = 0.3\,S/m$ is the conductivity of the extracellular medium, which we considered homogeneous.

The LFP at one point is the sum of the contributions from all the excitatory neurons in the entorhinal cortex and the hippocampus (dentate gyrus, CA3, and CA1): LFP=$\sum U$. In order to model the signal recorded by the macroscopic electrode and to compare it with real patient recordings, we averaged the LFP on two sets of 144 points evenly distributed on a cylinder of diameter 0.8mm going through the network, each of them representing a 2mm-long contact, separated by 1.5mm,and computed the difference between the two resulting signals, as in a bipolar sEEG montage (see figure 1-A). This bipolar montage was used in the patients recording so as to reduce the volume conduction (the influence of the neural activity of surrounding brain regions) on the signals.

Similarly to what was done in the intracerebral EEG recordings available to us (section 2.4), the simulated LFP was also bandpass filtered between 0.15Hz and 480Hz and downsampled to 1024Hz.

2.4 Inputs to the hippocampal model

The behavior of the model and its output are investigated under two different types of inputs, either stereotypical or realistic.

Stereotypical inputs are simply direct current injected into all excitatory and inhibitory neurons of the entorhinal cortex. To study the response of the model to input variations, we applied a square wave current I_{stim} starting at $t_0 = 250ms$ of which we varied the maximum value A_1 as well as the frequency f_1 across simulations:

$$I_{stim}(t) = \begin{cases} A_1 \text{ if } \{t > t_0 \text{ and } sin(2\pi f_1(t-t_0)) \geq 0\} \\ 0 \quad \text{otherwise.} \end{cases} \tag{4}$$

The amplitude of the input A_1 was chosen following our work in [Aussel et al., 2021] on the healthy hippocampus to best represent the slow-wave sleep ($A_1 = 1.2nA$) and wakefulness ($A_1 = 0.8nA$) behavior respectively.

Realistic inputs were simulated as synaptic inputs to the neurons of the entorhinal cortex, using excitatory synapses with the same conductance $g_{max,e}$ as within the network. Three groups of 10000 presynaptic neurons (assumed to belong to brain regions projecting onto the EC) were defined, each of the groups being connected to the neurons of a different slice of the entorhinal cortex with a uniform probability of 0.05. The presynaptic neurons were modeled as Poisson processes with variable firing rates (different for the three groups, but common within each group). In our realistic simulations, the varying Poisson firing rate was extracted from the envelope of real sEEG signals recorded in brain regions afferent to the hippocampus (see [Aussel et al., 2018] for details).

2.5 Clinical electrophysiological data

As mentioned at the beginning of this section, we aim to confront our model with real clinical data recorded using sEEG electrodes implanted in human epileptic subjects. In order to achieve this, real sEEG recorded signals were used both to create a realistic model input (as described in section 2.4) as well as to compare them with the LFP model output (section 2.3).

Fig. 2 Coregistered CT-MRI image showing the implantation of SEEG electrodes in a patient's hippocampi (frontal view).

The LFP data we used was obtained from one individual presenting mesio-temporal refractory epilepsy and implanted with deep intracerebral electrodes for surgery planning at the Neurology Service of the University Hospital (CHU) in Nancy, France. The patient gave an informed consent for using data for research purposes. The sEEG electrodes (Dixi Medical ®, France) had a diameter of 0.8mm, with 2mm-long contacts and 1.5mm inter-contact distance, 8 to 15 contacts per electrode. The patient was implanted according to phase 1 pre-surgical evaluation hypotheses notably in the left prefrontal cortex, left temporal lobe and in both hippocampi (see Figure 2 for an MRI reconstructed image of the bilateral hippocampal implantation). Left hippocampus was found as being the seizure onset zone. The position of the electrodes in the patient's brain was automatically ascertained using a procedure described in [Hofmanis et al., 2011].

The signals were recorded using Micromed®, Italy acquisition system. The sampling frequency was 1024 Hz. The signals of each patient were labelled by neurologists (OA) in order to identify the different stages of the sleep-wake cycle (based on synchronous surface EEG signal) as well as epileptic phenomena (interictal or seizures). Data from both the slow-wave sleep and wakefulness state was used.

2.6 Simulation tools

All the simulations were performed using the Brian2 libraries for Python ([Stimberg et al., 2014]), on the Grid'5000 testbed, supported by a scientific interest group hosted by Inria and including CNRS, RENATER and several Universities as well as other organizations (see `https://www.grid5000.fr`). The source code for the model is openly available on the ModelDB platform ([McDougal et al., 2016]), at : http://modeldb.yale.edu/266796.

2.7 Analysis method

We constructed our analysis in several steps.

2.7.1 Stereotypical inputs

Under stereotypical inputs, we have started by defining the output characteristics of interest. In [Aussel et al., 2021], we showed that our model is able to produce fast oscillatory patterns, with inter-pattern interval mostly (but not only) determined by the frequency of the stereotypical input. Since the human hippocampus is also able to produce both fast oscillations (gamma to fast ripple frequency range) and slow oscillations (delta to theta frequency range), we extract from the LFP output of the model two frequency characteristics:

- the mean frequency of the fast oscillatory patterns f_{fast}, i.e. the mean of the peak of the LFP spectrum in the 30-500Hz range (from gamma to ripple and higher) for each of the fast patterns
- the standard deviation of the frequency of the fast oscillatory patterns $std(f_{fast})$, i.e. the standard deviation of the peak of the LFP spectrum in the 30-500Hz range (from gamma to ripple and higher) for each of the fast patterns
- the peak frequency of LFP spectrum in the 1-30Hz range f_{slow} (from delta to gamma frequency, but also including the theta frequency band), which corresponds to the inter-pattern frequency

After a first evaluation of the behavior of the model, it appeared that the fastest oscillations were obtained for a square input of frequency $f_1 = 2.5Hz$. Therefore, this is the input frequency we use in section 3.1 to study the f_{fast} and $std(f_{fast})$ characteristics of the model. The f_{slow} characteristic on the other hand was studied by giving a constant input to the model and observing the natural frequency of the resulting slow oscillations.

To assess the significance of the f_{fast} and f_{slow} peaks in their respective frequency bands, we computed their Z-scores (i.e. the number of standard deviation above the mean of the spectrum in this frequency band they were reaching): for the fast oscillations all the peaks reported in the Results section reached a Z-score of at least 7.5, and for the slow oscillations all the peaks reported reached a Z-score of at least 4.5 (note that

lower Z-scores in the slow frequency band than in the fast frequency band due to the $1/f$ shape of brain activity). Therefore, all the selected peaks both in the fast and slow frequency bands were highly significant.

We have explored the space of the epileptic parameters (*spr*, *scl*, E_K and τ_{Cl}). The dimension being rather low, we could sample it regularly, performing a total of 648 five-second long simulations, testing six different values of the parameters *scl* and *spr* and three different values of the parameters E_K and τ_{Cl}, under the sleep and wakefulness conditions (we tested more different values of *scl* and *spr* compared to the other parameters as these appeared to have a more significant impact on the resulting oscillations) [1]. The results of these simulations are presented in section 3.1. They complement our previous work on the healthy hippocampus model at the basis of the present work [Aussel et al., 2021, Aussel et al., 2018].

2.7.2 Realistic setup

Once the healthy/epileptic models were systematically characterized using the stereotypical inputs, we immersed our model in a realistic context, by using realistic inputs and comparing it with the measured hippocampal sEEG signals. We performed 648 two-minute long simulations.

For generating the inputs, we extracted the envelope from the signals recorded by the electrodes located in the posterior inferior gyrus in prefrontal cortex, the inferior temporal gyrus in lateral temporal lobe and the temporal pole, and generated the Poisson spike trains as described above. The model output was compared with one sEEG seizure recorded in the left hippocampus, from the two most internal contacts of the electrode depicted in the right (radiological consensus) in figure 1-A.

For assessing the quality of the results under these simulations, we used characteristics more specific than simply the peaks in the high and low frequency bands f_{fast} and f_{slow}. More precisely, we focused on pathological oscillatory patterns associated with seizures and interictal epileptic discharges (IEDs).

In clinical context, seizures and IEDs are commonly detected by visual inspection of the EEG or sEEG signals by an expert. Their automated detection is still an active research field and often relies on machine learning techniques to cluster the data into a physiological and an epileptic set (see for example [Paul, 2018] for the detection of seizures or [Gaspard et al., 2014] for IEDs).

In this work, we chose to keep a classic clinical approach for the detection of pathological oscillations in our simulated signals in order to be able to verify them against real sEEG recorded seizure. Thus, seizure-like theta episodes were characterized by an increase in the power in the theta to alpha band (4-10Hz) as was shown being characteristic for hippocampus seizures by [Naftulin et al., 2018], [Perucca et al., 2014] in intracerebral recordings.

Interictal spikes, sharp-wave ripples, and fast ripples were detected by first filtering our simulated LFP in the corresponding frequency bands (10-80Hz, 120-200 Hz and 200-500Hz respectively), and computing the root mean square envelope (RMS) of the resulting signals. Events were then defined as portions of LFP with RMS higher than its mean value and with a peak at least four times its standard deviation in at least one of the defined frequency band. IEDs were defined as events with a peak in the RMS of the 10-80Hz filtered signal but no peak in the ripple or fast ripple frequency ranges, ripples were defined as events with a peak in the RMS of the 120- 200Hz filtered signal but no peak in the fast ripple frequency range, and fast ripples were defined as events with a peak in the RMS of the 200-500Hz filtered signal.

The analysis of the performances of the model in this realistic setup is presented in section 3.2.

3 Results

3.1 Exploration of the epilepsy parameter space under stereotypical inputs

In this section, we apply a stereotypical square-wave input to our network to study the frequency of the oscillations it can produce under different values of the epilepsy parameters (recall that 648 simulations were performed in total). It should be noted that though not all possible combinations of parameters are biologically plausible in a human hippocampus (for example, high mossy fiber sprouting with no hippocampal sclerosis), we are still sampling the complete parameter space in order to get a deeper understanding of the role of each parameter and their interactions. All simulations are done for both sleep and wakefulness conditions, i.e. after setting the parameters of the (healthy) hippocampus model at the values found in our previous works and recalled in Table 1. Similarly to the structural parameters that were chosen for one of the two conditions (sleep / wake), the input varied in amplitude, from high

[1] For an alternative way of assessing the role of different parameters in a higher dimensional parameter space, see [Aussel et al., 2021], where we analyzed the healthy hippocampus model.

amplitude for sleep ($A_1 = 1.2nA$) to lower amplitude ($A_1 = 0.8nA$) for wakefulness.

3.1.1 The pathological model produces altered oscillations under stereotypical inputs

Under stereotypical inputs, i.e. when stimulating entorhinal cortex neurons with a positive square current, the LFP generated by the network shows coupled fast and slow oscillations whose frequency varies with the pathological parameters.

The evolution of the fast oscillations peak frequency f_{fast} as a function of the four parameters *spr*, *scl*, E_K and τ_{Cl} is shown on Figure 3-A for slow-wave sleep and wakefulness respectively. Each subplot of this figure shows in color the values of f_{fast} depending on *spr* and *scl*, for fixed values of E_K and τ_{Cl}, which correspond to the line and column at which the subplot appears. The point in the bottom-left corner of the bottom-left plot therefore corresponds to a healthy hippocampus model. This layout will be used again throughout this article for the representation of other model outputs.

In both the slow-wave sleep and wakefulness modes, high mossy fiber sprouting level comes with higher frequency fast oscillations compared to the healthy hippocampus. Reciprocally, high hippocampal sclerosis tends to reduce the frequency of the fast oscillations produced by the network.

This study of f_{fast} suggests that the fast ripple oscillations observed in epileptic hippocampus experimentally in wakefulness and slow-wave sleep could be obtained in our model with high mossy fiber sprouting level and rather low sclerosis level. An hyperexcitability of the pyramidal neurons (controlled by the parameter E_K) would facilitate such pathological oscillations, especially in higher sclerosis settings. As for slower epileptiform patterns such as interictal discharges (of frequency typically less than $100Hz$), these could be obtained more easily with higher sclerosis levels and lower mossy fiber sprouting level. However it should be noted that the f_{fast} parameter does only reflect the highest peak in the power spectrum in the 30-500Hz frequency range and does not show if other significant peaks are present. This is why the presence of interictal activity will be assessed more precisely in the next section with realistic inputs.

The standard deviation of the f_{fast} frequency of the network activity emerging from ten successive stimulations is shown on Figure 3-B. From this, it can be noted that when presented with an input consisting of several stimulations with the same duration and amplitude, the network can respond with fast oscillatory patterns at different frequencies. This is especially true for intermediate to high values of the *scl*, *spr* and E_K parameters, that is when the network is at the limit between a healthy and a fast pathological behavior. The standard deviation of f_{fast} is also higher in the wakefulness compared to the slow-wave sleep state. Because no parameter was changed between successive simulations, it is likely that the different oscillatory frequencies result from a different initial state of the network when the stimulation starts (for example, the initial membrane potential of neurons, which are set randomly), and from the internal noise in the neuron models.

Epileptic features of the network influence the slow frequency of the oscillations f_{slow} as well (Figure 3-C). More precisely, medium sclerosis values coupled to healthy potassium dynamics enable the network to produce oscillations in the theta frequency band under constant input during both wakefulness and slow-wave sleep. Moreover, when potassium dynamics are altered the network is even able to produce activity in the alpha or low beta band with high sclerosis values.

It is interesting to notice that our experiments could in principle be used for predicting the output of the model for other parametrizations. Indeed, the relationship between the fast oscillations frequency f_{fast} and our four parameters can be estimated with a second order polynomial function (with a least-square method). This estimation yields a coefficient of determination R^2 [2] of 0.91 in the wakefulness mode and 0.89 in the slow-wave sleep one. In both sleep and wakefulness, one of the most important parameters is the mossy fiber sprouting level *spr*, but the sclerosis level *scl* and the potassium channel equilibrium potential E_K also play an important role, either on their own or squared or jointly with other parameters (see Figure 4). The chloride dynamics altered by the τ_{Cl} on the other hand only play a minimal role.

3.1.2 Model saturates in extreme high sprouting - low sclerosis conditions

Certain parameter values cause the network to saturate after a few seconds, i.e. to produce continuous paroxystic neural spiking in all the regions of the model, which does not stop even after all external input to the network is removed. This abnormal activity first arises from CA3, which can be expected knowing that this region is the one with highest recurrent excitation. The LFP in this saturated state shows a peak in the fast ripple frequency band (above 200Hz) in its spectrum.

[2] $R^2 = 1 - \frac{\sum_{i=1}^{N}(y_i - \hat{y}_i)^2}{\sum_{i=1}^{N}(y_i - \bar{y})^2}$ with y the observed values to estimate, $\bar{y}$ the mean of the observed values, $\hat{y}$ the modeled values and N the number of data points

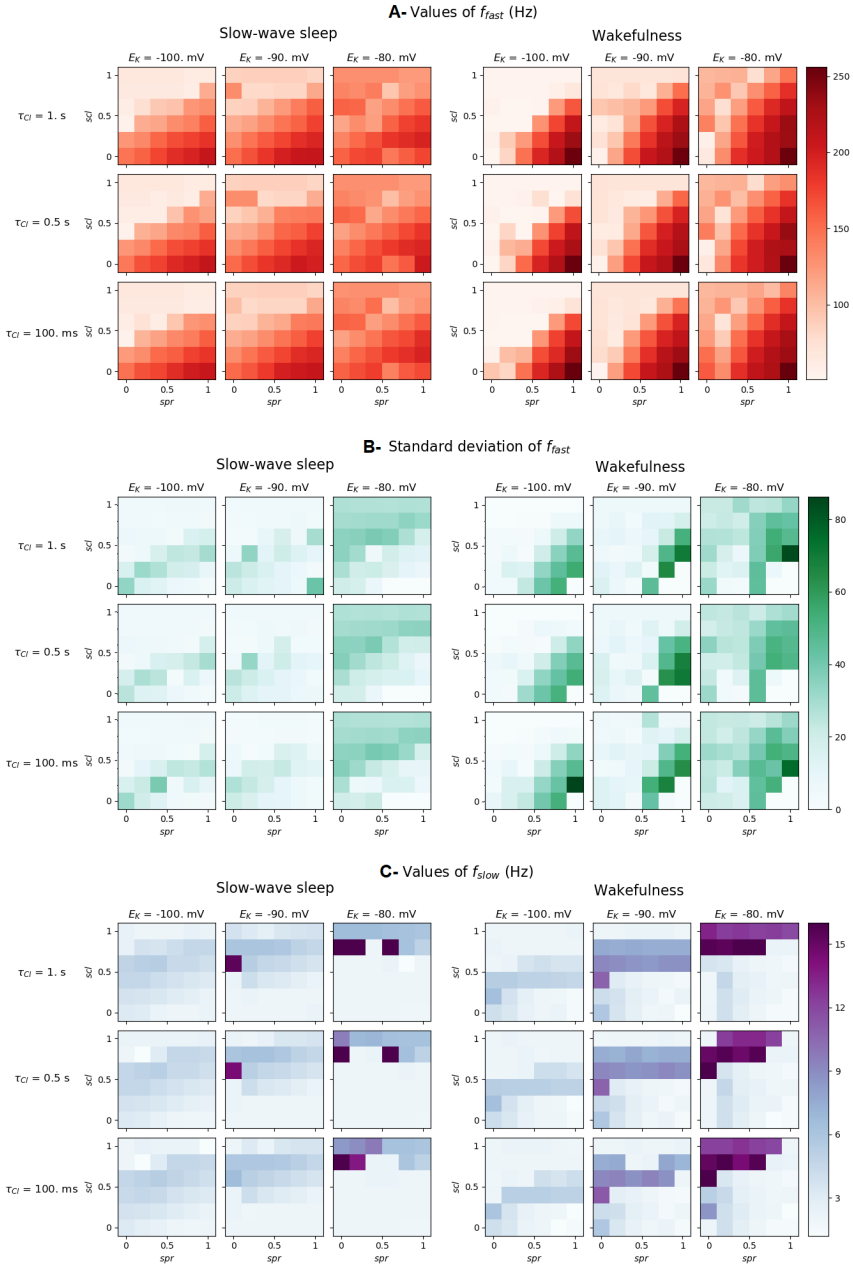

Fig. 3 Evolution of the frequency of the simulated LFP for different values of spr**,** scl**,** E_K **and** τ_{Cl}**.** A- Fast oscillation frequency f_{fast} under square input of amplitude A_1 and frequency f_1. **Fast oscillations frequency reaches abnormally high values during wakefulness for** $spr > scl$**.** B- Standard deviation of the fast oscillation frequency f_{fast} under square input of amplitude A_1 and frequency f_1. **Fast oscillations frequency varies when the network is presented with successive stimulations, all the more so with high** E_K**,** spr **and** scl**.** C- Slow oscillation frequency f_{slow} under constant input of amplitude A_1. **Under constant input, the network responds with slow oscillations in the delta to beta frequency band, higher** f_{slow} **values are obtained with high** E_K **and** scl**.** In each plot, the left panel shows results under slow-wave sleep settings, while the right panel shows wakefulness settings. The input stimulation has frequency $f_1 = 2.5Hz$ and amplitude $A_1 = 1.2nA$ for slow-wave sleep and $f_1 = 2.5Hz$ and $A_1 = 0.8nA$ for wakefulness.

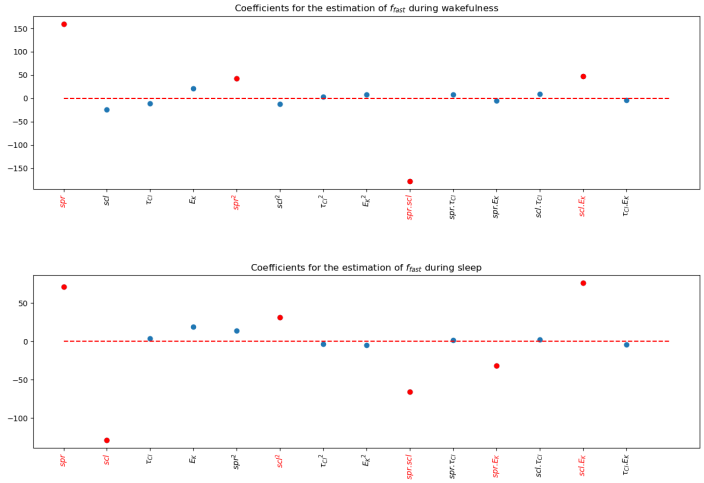

Fig. 4 Coefficients measuring each parameter's individual, squared or joint influence in the polynomial modeling of f_{fast} in the wakefulness (upper panel) and slow-wave sleep mode (lower panel). The significant coefficients (p<0.01) are shown in red.

Overall, results in the next sections should be interpreted with caution for areas of the parameter space leading to such paroxystic activity, although it should be noted that these areas (with excessive sprouting but little to no sclerosis) are unlikely to be seen in a human hippocampus in the first place.

Under wakefulness settings, such saturation state only appears with high mossy fiber sprouting level *spr* and low hippocampal sclerosis level *scl* ($(spr = 0.8, scl = 0)$,$(spr = 1, scl = 0)$ or $(spr = 1, scl = 0.2)$), which is consistent with an overall epileptogenic effect of sprouting ([Santhakumar et al., 2005]) compared to a protective effect of sclerosis ([Lopim et al., 2016]).

During slow-wave sleep, this phenomenon arises from a smaller subset of the parameters space, that is with high pyramidal cell hyperexcitability ($E_K = -80mV$ or higher), very high sprouting ($spr = 0.8$ or higher), and no hippocampal sclerosis ($scl = 0$). In conditions where instability appears only in wakefulness, it seems to arise from the modified synaptic connectivity accompanying wakefulness (and the increased excitatory synaptic strength in the dentate gyrus in particular), and not from the increased CAN current (see Figure S2).

3.2 Exploration of the pathological parameter space under realistic inputs

We next applied a realistic input to our network as defined in Section 2.4. More precisely, we chose portions of signal from a patient having a seizure episode during both slow-wave sleep and wakefulness to study the appearance of seizure-like theta episodes in our model, and portions of wakefulness and slow-wave sleep signal from another patient without seizures for the study of interictal events. It should be noted that, even though the LFP signals used to compute the input were recorded at the same time seizures or interictal events occurred in the hippocampus, they did not include any seizure nor interictal event themselves (as they were recorded in the prefrontal cortex, the lateral temporal lobe and the temporal pole, where no epileptic activity was present, according to medical expertise).

3.2.1 Seizure-like theta activity appears under balanced sclerosis and mossy fiber sprouting

Under wakefulness settings, it is possible for the model to reproduce high amplitude theta oscillations with similar temporal and frequency profile as in clinical seizure recordings, as shown on Figure 5-A-(a), except for the fact that simulated theta episodes do not stop (which is to be expected, since our model does not include any internal seizure termination mechanisms). Increasing the parameters *spr* or E_K, or decreasing the parameter *scl*, tends to increase the amplitude and frequency of the discharges in the seizure-like theta episode, to a point where the model produces permanent seizure-like theta discharges (i.e. that start at the very beginning of a simulation, independently of the input). Conversely, choosing parameters closer to a healthy state (Figure 5-A-(b)) reduces the amplitude of the discharges and the power in the theta band, to a point where the seizure-like theta disappears (the increase in theta band power at the start of the seizure being only due to an increase

of the amplitude of the inputs given to the model). It should also be noted that when stimulated with an input recorded outside a seizure episode, the pathological network produces isolated interictal events (see next section) but no seizure-like theta episodes, as shown on Figure 5-A-(c). In other words, both pathological epilepsy-related parameters and seizure-related inputs are needed for the model to reproduce this patient's seizure, which is why Figures 5-A-(b) and 5-A-(c) show little resemblance to the patient's seizure compared to Figure 5-A-(a).

The firing rates of the different neuron groups during the seizure-like theta episode with a pathological model are shown in Supplementary Figure S3 (and an animation is also provided in Supplementary Material), indicating that the theta patterns arise from synchronous neural spiking, starting from the EC and CA3 and then propagating to the DG and CA1. The seizure-like theta activity in the simulated LFP occurs when the input stimulation shows an increased power in the theta to beta frequency bands, in accordance with our previous results on stereotypical inputs. No significant change occurs in the spectrum of the simulated LFP before the beginning of the seizure-like theta episode.

The total power in the theta band in the whole seizure-like theta episode (Figure 5-B) is increased compared to a healthy network when the sclerosis parameter *scl* is smaller than the sprouting parameter *spr*, and is strongly reduced at higher sclerosis levels. The amount of the increase in theta power in this region of the parameter space is comparable to the clinical recordings available to us (i.e., the seizure episode shows an 11-fold increase in theta power compared to seizure-free recordings). Under wakefulness settings, the neuronal hyperexcitability controlled by E_K is slightly increasing the range of the *spr* and *scl* parameters enabling such high power in the theta band, thus making the network more prone to generate epileptiform theta activity. On the other hand, the slow-wave sleep network shows only a moderated increase of its theta band power in a highly sprouted compared to a healthy case, which shows that this vigilance state has a rather protective effect against seizure-like theta episodes.

3.2.2 Both single-cell and network level pathological parameters influence the production of interictal spikes and fast ripple activity

It is possible for the network to produce high amplitude, brief activity peaks similar to IEDs as shown on Figure 6-A. These interictal spikes tend to appear when a healthy slow-wave sleep network would produce large amplitude, slow oscillations (see Figure 6-B). They are more easily produced by a slow-wave sleep compared to a wakefulness network, especially when the sclerosis level *scl* is higher than the sprouting level *spr* (Figure 6-C). In wakefulness settings, the model predicts that impaired potassium dynamics (i.e. high E_K) enables the production of an increased number of IEDs in the high spouting, medium sclerosis region of the parameter space.

Though the increased number of IEDs in the $scl > spr$ region of the parameter space was to be expected in slow-wave sleep given our previous study of f_{fast} (Section 3.1), the lower number of IED in wakefulness is more surprising, but could be a consequence of the fact that even with a peak f_{fast} frequency in the gamma band, other faster oscillations also appear during high amplitude events (in other words the network produces fast ripples instead of IEDs, as will be shown thereafter).

The network is also able to reproduce fast ripples, i.e. transient events with peak frequency higher than physiological sharp-wave ripples (typically 200-500Hz), such as the example shown on Figure 7-A. These events can appear both in the slow-wave sleep and wakefulness modes, though they are more numerous in simulations in wakefulness settings (Figure 7-C). Wakefulness fast ripples can emerge from almost any combination of parameters, but are more numerous with high E_K or τ_{Cl} and $spr < scl$. On the other hand, the number of fast ripples under slow-wave sleep settings has a different profile, being more consistently produced in the $spr > scl$ region of the parameter space, especially with high τ_{Cl} and low E_K. In this figure, it should be noted that in the region where $E_K = -80mV$, *spr* is high and $scl = 0$, the network is in a saturated state (see section 3.1.2) and therefore fast ripple events cannot be reliably detected with our method, as oscillations within the fast ripple band are continuously produced.

Under slow-wave sleep settings, the three parameters *spr*, E_K and τ_{Cl} tend to increase the power in the fast ripple band (see Figure 7-B), while increased sclerosis *scl* reduce it. It should be noted that the increased power in the fast ripple band does not necessarily go with a decrease in the power in the ripple band, which is why the study of f_{fast} in Section 3.1 showed different results especially in the slow-wave sleep settings where sharp-wave ripples are prominent.

4 Discussion

In this work, we have modified our previously developed healthy hippocampal model ([Aussel et al., 2018]) into an epileptic model, so as to take into account four

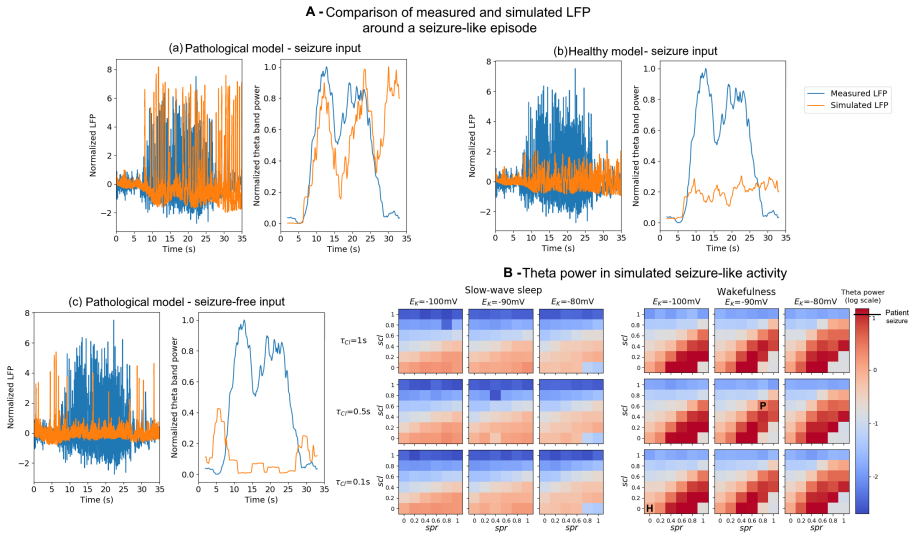

Fig. 5 Reproduction of seizure-like theta activity under realistic inputs. A-Comparison of the measured hippocampal LFP and its theta band power around a seizure in a patient (blue) and the simulated LFP of the model (orange). **Seizure-like theta oscillations are obtained with the model using epilepsy-related abnormalities and inputs drawn from a patient experiencing a seizure.** Example A-(a): With spr=0.8, scl=0.6, $E_K = -90mV$ and τ_{Cl}=0.5 second, and an input recorded during a seizure. Example A-(b): With a healthy model (spr=0, scl=0, $E_K = -100mV$ and τ_{Cl}=0.1 second), and an input recorded during a seizure. Example A-(c): With spr=0.8, scl=0.6, $E_K = -90mV$ and τ_{Cl}=0.5 second, and an input recorded outside a seizure. All LFPs were normalized so that their maximum value before the start of the seizure is equal to 1. B-Relative theta power of the simulated LFP compared to the healthy model, depending on the values of spr, scl, E_K and τ_{Cl}, under sleep (left) or wakefulness (right) settings. The values shown are in log-scale, with the zero corresponding to the theta band power in healthy conditions. The relative theta power of the individual with epilepsy in an epoch containing a seizure compared to a seizure-free epoch is indicated on the color bar. The parameter values corresponding to the pathological and healthy examples shown on panel A are indicated with the letters P and H respectively. **High theta power close to patient's seizure can be obtained with the model under wakefulness settings and $spr > scl$.**

hippocampal abnormalities usually associated with epilepsy, that is hippocampal sclerosis (type I), mossy fiber sprouting, impaired potassium dynamics (leading to neuronal hyperexcitability), and impaired chloride dynamics (leading to impaired inhibition).

These pathological features include both network and single-cell dynamics for excitatory neurons, but it should be noted that our model does not involve interneuron pathologies, which may play a peculiar role in epilepsy and seizure onset ([Chang et al., 2018], [Rich et al., 2020]), as inhibition typically increases synchrony in neuronal networks ([Diba et al., 2014]). Also, our model does not tackle seizure initiation or termination mechanisms, such as synaptic depletion (see the review from [Lado and Moshé, 2008]). Such features will be left for future works.

A study of the network's behavior under stereotypical inputs reveals that very fast oscillations, as well as saturation, can now be obtained, which was not possible with the "healthy" model described in our previous works ([Aussel et al., 2021]). The wakefulness state enhances the capacity of the network to produce such saturated state, mostly due to the combined effects of mossy fiber sprouting and cholinergic modulation of synaptic currents. Impaired potassium dynamics also favor such abnormal activities, while hippocampal sclerosis has a rather protective effect.

When stimulated with a realistic input, the modeled network can also reproduce theta oscillations characteristic of epileptic seizures as well as interictal spikes and fast ripples. The timing of epileptic seizure-like theta rhythms is in particular determined by the power in the theta to beta frequency ranges in the stimulation input given to the network.

Modeled seizure-like theta patterns closest to the clinically recorded seizures can be obtained when the degrees of sclerosis and mossy fiber sprouting are properly balanced. High mossy fiber sprouting with low hippocampal sclerosis leads to perpetual seizure-like theta activity, while high sclerosis with low sprouting suppresses the theta patterns. Interestingly, impaired potassium and chloride dynamics have little influence on the generation of theta seizures-like oscillations (at least not directly, though the increased excitability and fast spiking they induce can increase neuronal death through excitotoxicity, see [Wang and Qin, 2010] or [Deshpande et al., 2007], and can be involved in epileptogenesis). In accordance with clinical observations (see [Crespel et al., 1998] or [Sedigh-Sarvestani et al., 2014]), and as our study under stereotypical inputs

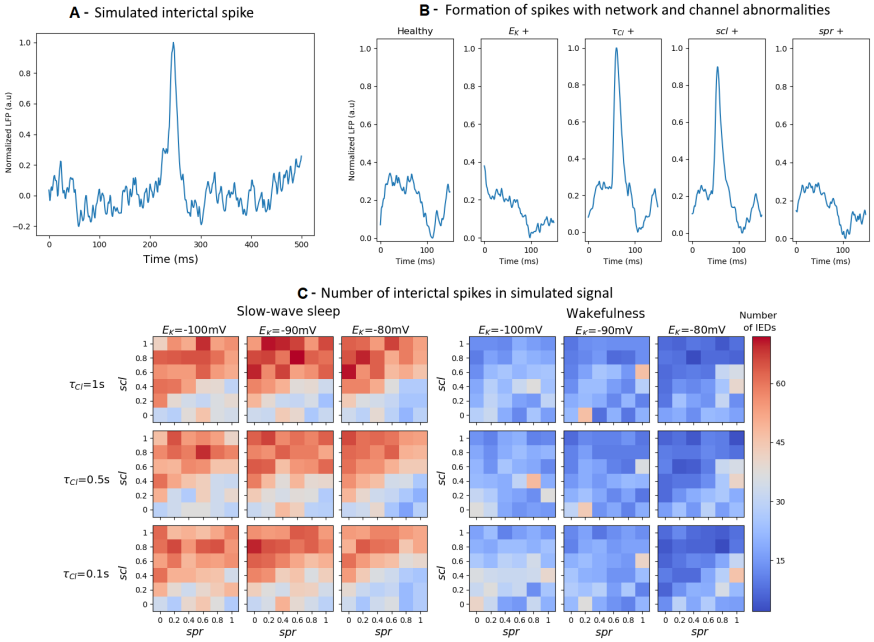

Fig. 6 Interictal epileptiform discharges generated by the model. A- Example of an interictal discharge simulated with a network in a slow-wave sleep state with $spr = 0.6$, $scl = 0.6$, $E_K = -90mV$ and $\tau_{Cl} = 500ms$. B- Comparison of the LFP generated with a network in a slow-wave sleep state in five different conditions, under the same input stimulation. Healthy state : $spr = 0$, $scl = 0$, $E_K = -100mV$ and $\tau_{Cl} = 100ms$. E_K + state : $spr = 0$, $scl = 0$, $E_K = -80mV$ and $\tau_{Cl} = 100ms$. τ_{Cl} + state : $spr = 0$, $scl = 0$, $E_K = -100mV$ and $\tau_{Cl} = 1s$. scl + state : $spr = 0$, $scl = 0.2$, $E_K = -100mV$ and $\tau_{Cl} = 100ms$. spr + state : $spr = 0.2$, $scl = 0$, $E_K = -100mV$ and $\tau_{Cl} = 100ms$. **Increased τ_{Cl} or scl give rise to an interictal discharge.** C- Number of interictal discharges obtained with a network under slow-wave sleep (left) or wakefulness (right) settings in a one-minute-long simulation for different values of spr, scl, E_K and τ_{Cl}. **Highest number of interictal spikes can be obtained with the model under slow-wave sleep settings and $spr < scl$.**

suggested, theta oscillation characteristic of seizures are more prominent in the model of wakefulness compared to slow-wave sleep.

In the pathological model, interictal spikes are more commonly produced under slow-wave sleep settings than under wakefulness, especially in the presence of hippocampal sclerosis. However, they can also be produced during both sleep and wakefulness under impaired potassium dynamics. Fast ripples on the other hand are more commonly produced by the model during wakefulness, but are also slightly favored during slow-wave sleep if chloride dynamics are impaired. One possible consequence of these results is that cognitive impairments seen in individuals with epilepsy, and promoted by interictal spikes and fast ripples ([Kleen et al., 2013], [Krauss et al., 1997]), might be reduced by targeting such chloride and potassium mechanisms. This hypothesis could be further supported by experiments conducted in mice where Kv1.1 ion channels are affected ([Thouta et al., 2021] in the amygdala).

Overall, we observed that the $spr = scl$ hyperplane of the parameter space plays a very important role in the production of pathological oscillations. With high spr and scl, it is possible to reproduce realistic seizure-like theta oscillations as well as numerous fast ripple oscillations during wakefulness. During slow-wave sleep $scl > spr$ increases the number of interictal discharges while $spr > scl$ favors fast ripple oscillations. Impaired potassium and chloride dynamics mostly influence the generation of interictal discharges and fast ripples, but not the generation of seizure-like theta activity (in the parameter range we studied). Seizure-like theta episodes are mostly the result of the abnormal structural connectivity induced by mossy fiber sprouting and specific functional connectivity of wakefulness. This is important as the role of mossy fiber sprouting in epileptogenesis is debated ([Elmér et al., 1997]). Our results are in accordance with ([Isokawa et al., 1993]) and plead for a major role of mossy fiber spouting in seizure genesis. This supports further research on mossy fiber sprouting as potential therapeutic target for mesial temporal lobe epilepsy ([Cavarsan et al., 2018]). More, as mossy fiber normal synaptogenesis was shown to be related to long term spatial memory ([Ramírez-Amaya et al., 2001]), higher rates of aberrant sprouting (as found in our study) may support memory impairments found in individuals with medial temporal epilepsy. Finally,

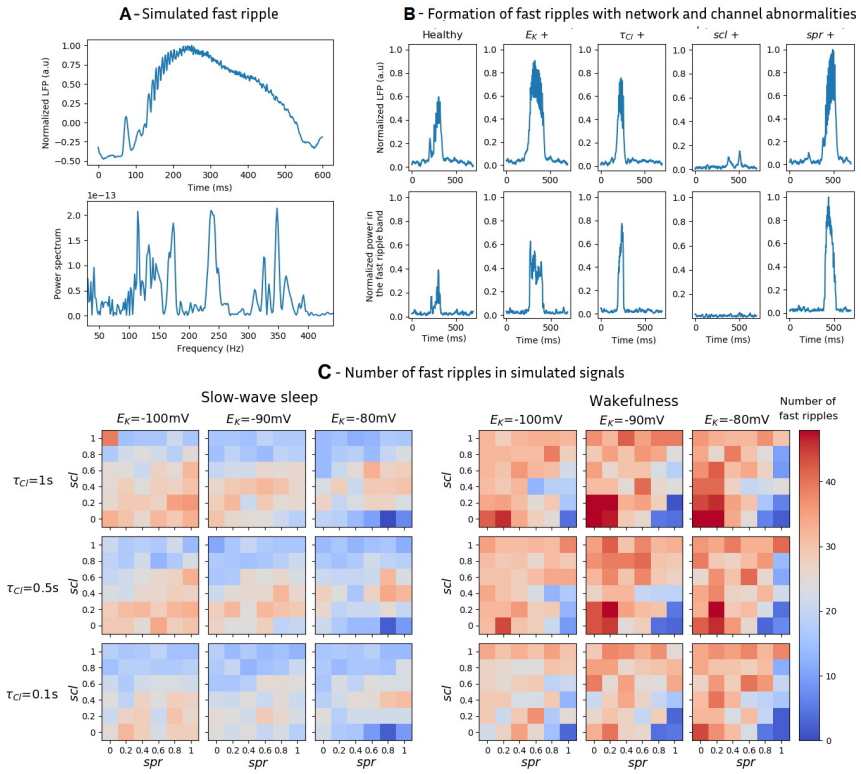

Fig. 7 Fast ripples generated by the network. A- Example of a fast ripple simulated with a network in a slow-wave sleep state with $spr = 0$, $scl = 0$, $E_K = -90mV$ and $\tau_{Cl} = 100ms$, showing raw LFP trace (top) and power spectrum (bottom). B-Comparison of the activity generated with a network in a slow-wave sleep state in five different conditions, under the same input stimulation generating a sharp-wave ripple like event, showing raw LFP traces (top) and power in the fast ripples frequency band (bottom). Healthy state : $spr = 0$, $scl = 0$, $E_K = -100mV$ and $\tau_{Cl} = 100ms$. E_K + state : $spr = 0$, $scl = 0$, $E_K = -80mV$ and $\tau_{Cl} = 100ms$. τ_{Cl} + state : $spr = 0$, $scl = 0$, $E_K = -100mV$ and $\tau_{Cl} = 1s$. scl + state : $spr = 0$, $scl = 0.2$, $E_K = -100mV$ and $\tau_{Cl} = 100ms$. spr + state : $spr = 0.2$, $scl = 0$, $E_K = -100mV$ and $\tau_{Cl} = 100ms$. **Parameters** spr**,** E_K **and** τ_{Cl} **increase the power in the fast ripple band of healthy sharp-wave ripple complexes while** scl **decreases it.** C-Number of fast ripple oscillations obtained with a network under slow-wave sleep (left) or wakefulness (right) settings in a one-minute-long simulation for different values of spr, scl, E_K and τ_{Cl}. **Highest number of fast ripples can be obtained with the model under wakefulness settings with high** E_k **and** τ_{Cl} **and** $spr < scl$**.**

our study of interictal spikes and fast ripples shows the importance of inhibition in spiking synchrony enhancement (as previous modeling studies [Giovannini et al., 2017]). Therefore, large inhibition may lead to high synchrony which in turn could yield increased mossy fiber sprouting, and so on. This further suggests that pharmacological treatments aiming at reinforcing gabaergic inhibition that are largely used in clinical approaches may not be the most suitable strategies to avoid epilepsies which are, by definition, the behavioral expression of abnormal synchronized neuronal activity.

5 Declarations

5.1 Funding

The authors have no funding to declare.

5.2 Conflicts of Interest

The authors have no conflicts of interest to declare.

5.3 Availability of data and code

All the Python source files used for building the network and running the simulations are accessible on the ModelDB public repositories.

5.4 Author Contributions

AA, LB and RR designed the study. SCC, LT and LM collected the sEEG data. AA built the computational model and performed the simulations. AA, LB, OA and RR analyzed the results. AA drafted the paper. All authors approved the final manuscript.

References

Andersen et al., 2007. Andersen, P., Morris, R., Amaral, D., Bliss, T., and O'Keefe, J. (2007). *The hippocampus book*. Oxford University Press.

Asadi-Pooya et al., 2017. Asadi-Pooya, A. A., Stewart, G. R., Abrams, D. J., and Sharan, A. (2017). Prevalence and incidence of drug-resistant mesial temporal lobe epilepsy in the United States. *World Neurosurgery*, 99:662–666.

Auer et al., 2020. Auer, T., Schreppel, P., Erker, T., and Schwarzer, C. (2020). Impaired chloride homeostasis in epilepsy: Molecular basis, impact on treatment, and current treatment approaches. *Pharmacology & Therapeutics*, 205:107422.

Aussel et al., 2021. Aussel, A., Buhry, L., and Ranta, R. (2021). Design of experiments and sobol' sensitivity analysis of a hippocampus computational model. In *2021 43rd Annual International Conference of the IEEE Engineering in Medicine Biology Society (EMBC)*, pages 6146–6150.

Aussel et al., 2018. Aussel, A., Buhry, L., Tyvaert, L., and Ranta, R. (2018). A detailed anatomical and mathematical model of the hippocampal formation for the generation of sharp-wave ripples and theta-nested gamma oscillations. *Journal of Computational Neuroscience*, 45(3):207–221.

Babb et al., 1989. Babb, T., Pretorius, J., Kupfer, W., and Crandall, P. (1989). Glutamate decarboxylase-immunoreactive neurons are preserved in human epileptic hippocampus. *The Journal of Neuroscience*, 9(7):2562–2574.

Bausch and McNamara, 2000. Bausch, S. B. and McNamara, J. O. (2000). Synaptic connections from multiple subfields contribute to granule cell hyperexcitability in hippocampal slice cultures. *Journal of Neurophysiology*, 84(6):2918–2932.

Blümcke et al., 2013. Blümcke, I., Thom, M., Aronica, E., Armstrong, D. D., Bartolomei, F., Bernasconi, A., Bernasconi, N., Bien, C. G., Cendes, F., Coras, R., Cross, J. H., Jacques, T. S., Kahane, P., Mathern, G. W., Miyata, H., Moshé, S. L., Oz, B., Özkara, Ç., Perucca, E., Sisodiya, S., Wiebe, S., and Spreafico, R. (2013). International consensus classification of hippocampal sclerosis in temporal lobe epilepsy: A task force report from the ILAE commission on diagnostic methods. *Epilepsia*, 54(7):1315–1329.

Buckmaster et al., 2002. Buckmaster, P. S., Zhang, G. F., and Yamawaki, R. (2002). Axon sprouting in a model of temporal lobe epilepsy creates a predominantly excitatory feedback circuit. *The Journal of Neuroscience*, 22(15):6650–6658.

Cavarsan et al., 2018. Cavarsan, C. F., Malheiros, J., Hamani, C., Najm, I., and Covolan, L. (2018). Is mossy fiber sprouting a potential therapeutic target for epilepsy? *Frontiers in Neurology*, 9.

Chamma et al., 2012. Chamma, I., Chevy, Q., Poncer, J. C., and Lévi, S. (2012). Role of the neuronal k-cl co-transporter KCC2 in inhibitory and excitatory neurotransmission. *Frontiers in Cellular Neuroscience*, 6.

Chang et al., 2018. Chang, M., Dian, J. A., Dufour, S., Wang, L., Chameh, H. M., Ramani, M., Zhang, L., Carlen, P. L., Womelsdorf, T., and Valiante, T. A. (2018). Brief activation of GABAergic interneurons initiates the transition to ictal events through post-inhibitory rebound excitation. *Neurobiology of Disease*, 109:102–116.

Coulter and Steinhauser, 2015. Coulter, D. A. and Steinhauser, C. (2015). Role of astrocytes in epilepsy. *Cold Spring Harbor Perspectives in Medicine*, 5(3):a022434–a022434.

Crespel et al., 1998. Crespel, A., Baldy-Moulinier, M., and Coubes, P. (1998). The relationship between sleep and epilepsy in frontal and temporal lobe epilepsies: Practical and physiopathologic considerations. *Epilepsia*, 39(2):150–157.

Cressman et al., 2009. Cressman, J. R., Ullah, G., Ziburkus, J., Schiff, S. J., and Barreto, E. (2009). The influence of sodium and potassium dynamics on excitability, seizures, and the stability of persistent states: I. Single neuron dynamics. *Journal of Computational Neuroscience*, 26(2):159–170.

Demont-Guignard et al., 2009. Demont-Guignard, S., Benquet, P., Gerber, U., and Wendling, F. (2009). Analysis of intracerebral EEG recordings of epileptic spikes: Insights from a neural network model. *IEEE Transactions on Biomedical Engineering*, 56(12):2782–2795.

Deshpande et al., 2007. Deshpande, L. S., Lou, J. K., Mian, A., Blair, R. E., Sombati, S., and DeLorenzo, R. J. (2007). In vitro status epilepticus but not spontaneous recurrent seizures cause cell death in cultured hippocampal neurons. *Epilepsy Research*, 75(2-3):171–179.

Diba et al., 2014. Diba, K., Amarasingham, A., Mizuseki, K., and Buzsaki, G. (2014). Millisecond timescale synchrony among hippocampal neurons. *Journal of Neuroscience*, 34(45):14984–14994.

Dyhrfjeld-Johnsen, 2008. Dyhrfjeld-Johnsen, J. (2008). Upregulated h-current in hyperexcitable CA1 dendrites after febrile seizures. *Frontiers in Cellular Neuroscience*, 2.

Elmér et al., 1997. Elmér, E., Kokaia, Z., Kokaia, M., Lindvall, O., and McIntyre, D. C. (1997). Mossy fibre sprouting: evidence against a facilitatory role in epileptogenesis. *Neuroreport*, 8(5):1193–1196.

Fisher et al., 2014. Fisher, R. S., Acevedo, C., Arzimanoglou, A., Bogacz, A., Cross, J. H., Elger, C. E., Engel, J., Forsgren, L., French, J. A., Glynn, M., Hesdorffer, D. C., Lee, B., Mathern, G. W., Moshé, S. L., Perucca, E., Scheffer, I. E., Tomson, T., Watanabe, M., and Wiebe, S. (2014). ILAE official report: A practical clinical definition of epilepsy. *Epilepsia*, 55(4):475–482.

Fritschy et al., 1999. Fritschy, J.-M., Kiener, T., Bouilleret, V., and Loup, F. (1999). GABAergic neurons and GABAA-receptors in temporal lobe epilepsy. *Neurochemistry International*, 34(5):435–445.

Gaspard et al., 2014. Gaspard, N., Alkawadri, R., Farooque, P., Goncharova, I. I., and Zaveri, H. P. (2014). Automatic detection of prominent interictal spikes in intracranial EEG: Validation of an algorithm and relationsip to the seizure onset zone. *Clinical Neurophysiology*, 125(6):1095–1103.

Gelinas et al., 2016. Gelinas, J. N., Khodagholy, D., Thesen, T., Devinsky, O., and Buzsáki, G. (2016). Interictal epileptiform discharges induce hippocampal–cortical coupling in temporal lobe epilepsy. *Nature Medicine*, 22(6):641–648.

Giovannini et al., 2017. Giovannini, F., Knauer, B., Yoshida, M., and Buhry, L. (2017). The can-in network: A biologically inspired model for self-sustained theta oscillations and memory maintenance in the hippocampus. *Hippocampus*, 27(4):450–463.

Hofmanis et al., 2011. Hofmanis, J., Caspary, O., Louis-Dorr, V., and Maillard, L. (2011). Automatic depth electrode localization in intracranial space. In *4th International Conference on Bio-inspired Systems and Signal Processing, Biosignals 2011*, page CDROM, Rome, Italy.

Huberfeld et al., 2007. Huberfeld, G., Wittner, L., Clemenceau, S., Baulac, M., Kaila, K., Miles, R., and Rivera, C. (2007). Perturbed chloride homeostasis and GABAergic signaling in human temporal lobe epilepsy. *Journal of Neuroscience*, 27(37):9866–9873.

Isokawa et al., 1993. Isokawa, M., Levesque, M., Babb, T., and Engel, J. (1993). Single mossy fiber axonal systems of

human dentate granule cells studied in hippocampal slices from patients with temporal lobe epilepsy [published erratum appears in j neurosci 1993 jun;13(6):following table of contents]. *Journal of Neuroscience*, 13(4):1511–1522.

Jinno and Kosaka, 2010. Jinno, S. and Kosaka, T. (2010). Stereological estimation of numerical densities of glutamatergic principal neurons in the mouse hippocampus. *Hippocampus*, 20(7):829–840.

Jiruska et al., 2014. Jiruska, P., De Curtis, M., and Jefferys, J. G. (2014). *Modern concepts of focal epileptic networks*. Elsevier.

Jiruska et al., 2013. Jiruska, P., de Curtis, M., Jefferys, J. G. R., Schevon, C. A., Schiff, S. J., and Schindler, K. (2013). Synchronization and desynchronization in epilepsy: controversies and hypotheses. *The Journal of Physiology*, 591(4):787–797.

Jochems and Yoshida, 2015. Jochems, A. and Yoshida, M. (2015). A robust in vivo-like persistent firing supported by a hybrid of intracellular and synaptic mechanisms. *PLOS ONE*, 10(4):e0123799.

Kleen et al., 2013. Kleen, J. K., Scott, R. C., Holmes, G. L., Roberts, D. W., Rundle, M. M., Testorf, M., Lenck-Santini, P.-P., and Jobst, B. C. (2013). Hippocampal interictal epileptiform activity disrupts cognition in humans. *Neurology*, 81(1):18–24.

Krauss et al., 1997. Krauss, G. L., Summerfield, M., Brandt, J., Breiter, S., and Ruchkin, D. (1997). Mesial temporal spikes interfere with working memory. *Neurology*, 49(4):975–980.

Lado and Moshé, 2008. Lado, F. A. and Moshé, S. L. (2008). How do seizures stop? *Epilepsia*, 49(10):1651–1664.

Lerche et al., 2012. Lerche, H., Shah, M., Beck, H., Noebels, J., Johnston, D., and Vincent, A. (2012). Ion channels in genetic and acquired forms of epilepsy. *The Journal of Physiology*, 591(4):753–764.

Liou et al., 2020. Liou, J., Smith, E. H., Bateman, L. M., Bruce, S. L., McKhann, G. M., Goodman, R. R., Emerson, R. G., Schevon, C. A., and Abbott, L. (2020). A model for focal seizure onset, propagation, evolution, and progression. *eLife*, 9.

Lopim et al., 2016. Lopim, G. M., Campos, D. V., da Silva, S. G., de Almeida, A. A., Lent, R., Cavalheiro, E. A., and Arida, R. M. (2016). Relationship between seizure frequency and number of neuronal and non-neuronal cells in the hippocampus throughout the life of rats with epilepsy. *Brain Research*, 1634:179–186.

Mazzoni et al., 2015. Mazzoni, A., Lindén, H., Cuntz, H., Lansner, A., Panzeri, S., and Einevoll, G. T. (2015). Computing the local field potential (lfp) from integrate-and-fire network models. *PLOS Computational Biology*, 11(12):1–38.

McDougal et al., 2016. McDougal, R. A., Morse, T. M., Carnevale, T., Marenco, L., Wang, R., Migliore, M., Miller, P. L., Shepherd, G. M., and Hines, M. L. (2016). Twenty years of ModelDB and beyond: building essential modeling tools for the future of neuroscience. *Journal of Computational Neuroscience*, 42(1):1–10.

Morgan and Soltesz, 2008. Morgan, R. J. and Soltesz, I. (2008). Nonrandom connectivity of the epileptic dentate gyrus predicts a major role for neuronal hubs in seizures. *Proceedings of the National Academy of Sciences*, 105(16):6179–6184.

Naftulin et al., 2018. Naftulin, J. S., Ahmed, O. J., Piantoni, G., Eichenlaub, J.-B., Martinet, L.-E., Kramer, M. A., and Cash, S. S. (2018). Ictal and preictal power changes outside of the seizure focus correlate with seizure generalization. *Epilepsia*, 59(7):1398–1409.

Netoff, 2004. Netoff, T. I. (2004). Epilepsy in small-world networks. *Journal of Neuroscience*, 24(37):8075–8083.

Noebels et al., 2012. Noebels, J. L., Avoli, M., Rogawski, M. A., Olsen, R. W., Delgado-Escueta, A. V., and Buckmaster, P. S. (2012). *Jasper's Basic Mechanisms of Epilepsies*. Oxford University Press.

O'Leary et al., 2013. O'Leary, T., Williams, A. H., Caplan, J. S., and Marder, E. (2013). Correlations in ion channel expression emerge from homeostatic tuning rules. *Proceedings of the National Academy of Sciences*, 110(28):E2645–E2654.

Pathak et al., 2007. Pathak, H. R., Weissinger, F., Terunuma, M., Carlson, G. C., Hsu, F.-C., Moss, S. J., and Coulter, D. A. (2007). Disrupted dentate granule cell chloride regulation enhances synaptic excitability during development of temporal lobe epilepsy. *Journal of Neuroscience*, 27(51):14012–14022.

Patton and McNaughton, 1995. Patton, P. E. and McNaughton, B. (1995). Connection matrix of the hippocampal formation: I. The dentate gyrus. *Hippocampus*, 5(4):245–286.

Paul, 2018. Paul, Y. (2018). Various epileptic seizure detection techniques using biomedical signals: a review. *Brain Informatics*, 5(2).

Perucca et al., 2014. Perucca, P., Dubeau, F., and Gotman, J. (2014). Intracranial electroencephalographic seizure-onset patterns: effect of underlying pathology. *Brain*, 137(1):183–196. Publisher: Oxford Academic.

Pettersen et al., 2012. Pettersen, K. H., Lindén, H., Dale, A. M., and Einevoll, G. T. (2012). Extracellular spikes and CSD. *Handbook of neural activity measurement*, 1:92–135.

Ramírez-Amaya et al., 2001. Ramírez-Amaya, V., Balderas, I., Sandoval, J., Escobar, M. L., and Bermúdez-Rattoni, F. (2001). Spatial long-term memory is related to mossy fiber synaptogenesis. *Journal of Neuroscience*, 21(18):7340–7348.

Ratnadurai Giridharan et al., 2014. Ratnadurai Giridharan, S., Stefanescu, R., Khargonekar, P., Carney, P., and Talathi, S. (2014). Genesis of interictal spikes in the ca1: a computational investigation. *Frontiers in Neural Circuits*, 8:2.

Rich et al., 2022. Rich, S., Chameh, H. M., Lefebvre, J., and Valiante, T. A. (2022). Loss of neuronal heterogeneity in epileptogenic human tissue impairs network resilience to sudden changes in synchrony. *Cell Reports*, 39(8):110863.

Rich et al., 2020. Rich, S., Chameh, H. M., Rafiee, M., Ferguson, K., Skinner, F. K., and Valiante, T. A. (2020). Inhibitory network bistability explains increased interneuronal activity prior to seizure onset. *Frontiers in Neural Circuits*, 13.

Santhakumar et al., 2005. Santhakumar, V., Aradi, I., and Soltesz, I. (2005). Role of mossy fiber sprouting and mossy cell loss in hyperexcitability: A network model of the dentate gyrus incorporating cell types and axonal topography. *Journal of Neurophysiology*, 93(1):437–453.

Sedigh-Sarvestani et al., 2014. Sedigh-Sarvestani, M., Thuku, G. I., Sunderam, S., Parkar, A., Weinstein, S. L., Schiff, S. J., and Gluckman, B. J. (2014). Rapid eye movement sleep and hippocampal theta oscillations precede seizure onset in the tetanus toxin model of temporal lobe epilepsy. *Journal of Neuroscience*, 34(4):1105–1114.

Stefanescu et al., 2012. Stefanescu, R. A., Shivakeshavan, R., and Talathi, S. S. (2012). Computational models of epilepsy. *Seizure*, 21(10):748–759.

Stimberg et al., 2014. Stimberg, M., Goodman, D. F., Benichoux, V., and Brette, R. (2014). Equation-oriented specification of neural models for simulations. *Frontiers in Neuroinformatics*, 8.

Tejada and Roque, 2014. Tejada, J. and Roque, A. C. (2014). Computational models of dentate gyrus with epilepsy-induced morphological alterations in granule cells. *Epilepsy and Behavior*, 38:63–70.

Thouta et al., 2021. Thouta, S., Zhang, Y., Garcia, E., and Snutch, T. (2021). Kv1.1 channels mediate network excitability and feed-forward inhibition in local amygdala circuits. *Scientific Reports*, 11.

van den Heuvel et al., 2019. van den Heuvel, M. P., Scholtens, L. H., and Kahn, R. S. (2019). Multiscale neuroscience of psychiatric disorders. *Biological Psychiatry*, 86(7):512–522.

Wang and Qin, 2010. Wang, Y. and Qin, Z. (2010). Molecular and cellular mechanisms of excitotoxic neuronal death. *Apoptosis*, 15(11):1382–1402.

Wendling et al., 2002. Wendling, F., Bartolomei, F., Bellanger, J. J., and Chauvel, P. (2002). Epileptic fast activity can be explained by a model of impaired GABAergic dendritic inhibition. *European Journal of Neuroscience*, 15(9):1499–1508.

Wendling et al., 2012. Wendling, F., Bartolomei, F., Mina, F., Huneau, C., and Benquet, P. (2012). Interictal spikes, fast ripples and seizures in partial epilepsies - combining multi-level computational models with experimental data. *European Journal of Neuroscience*, 36(2):2164–77.

West and Gundersen, 1990. West, M. J. and Gundersen, H. J. G. (1990). Unbiased stereological estimation of the number of neurons in the human hippocampus. *The Journal of Comparative Neurology*, 296(1):1–22.

S1 Supplementary Material : Modeling hippocampal sclerosis as a loss of both interneurons and excitatory neurons

S2 Supplementary Material : Saturating network

S3 Supplementary Material : Firing rates during a modeled seizure-like theta episode

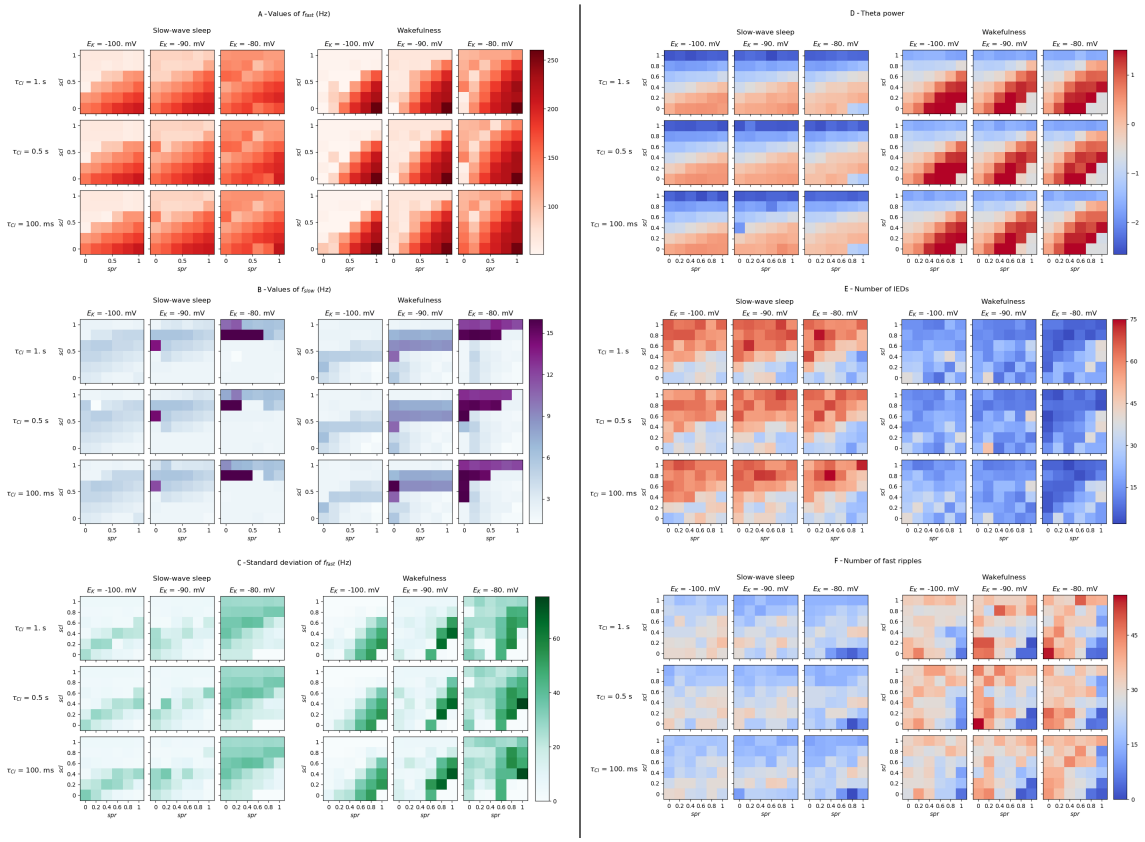

Fig. S1 Evaluation of the model with sclerosis (*scl* parameter) reducing the number of interneurons in the same proportion as excitatory neurons. On each panel (A to F), an output of the model is evaluated depending on the values of *spr*, *scl*, E_K and τ_{Cl}, under sleep (left) or wakefulness (right) settings. A- Fast oscillation frequency f_{fast} under stereotypical inputs. B- Slow oscillation frequency f_{slow} under stereotypical inputs. C- Standard deviation of the fast oscillation frequency f_{fast} under stereotypical inputs. D- Relative theta power of the simulated LFP compared to the healthy model (log scale) under realistic inputs. E- Number of interictal discharges under realistic inputs. F- Number of fast ripples under realistic inputs

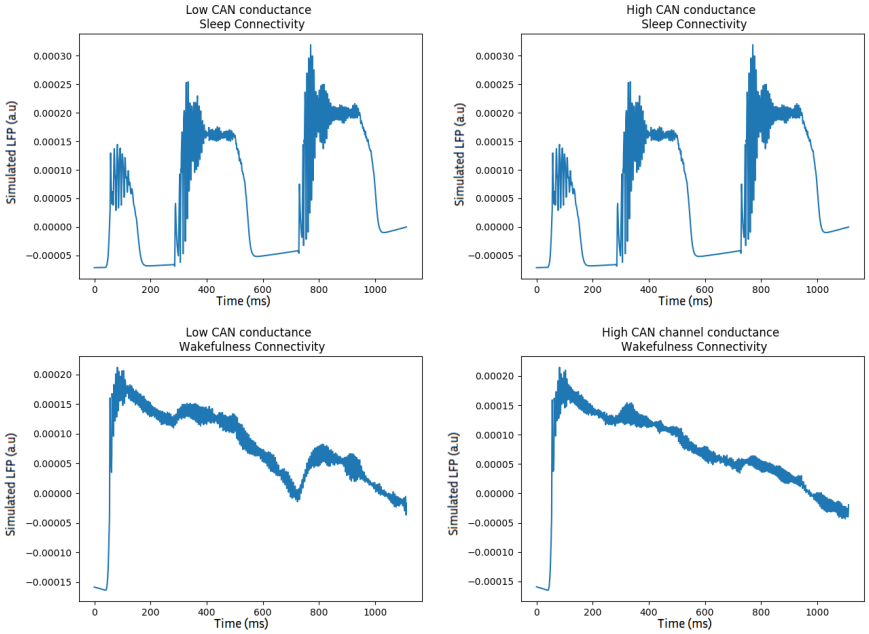

Fig. S2 Network saturation appears with high sprouting and low sclerosis levels. Simulated LFP under a square current of amplitude 1nA, with $spr = 1$, $scl = 0.2$, $E_K = -100mV$ and $\tau_{Cl} = 0.01s$, with low or high CAN channel conductance and wakefulness or slow-wave sleep connectivity. The network saturates only with wakefulness connectivity.

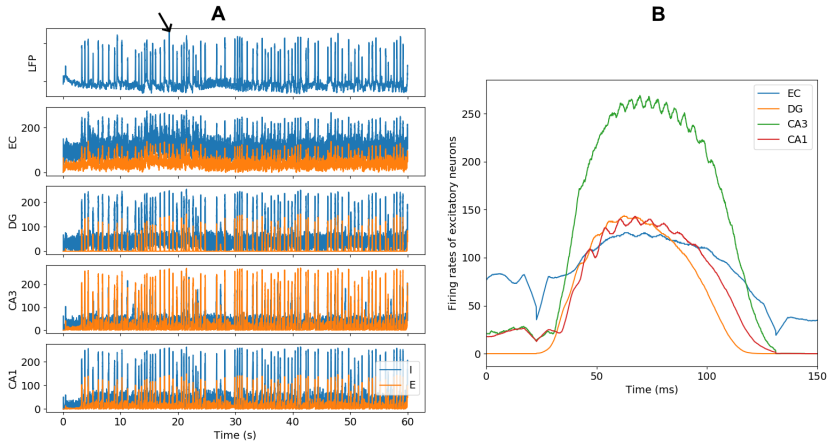

Fig. S3 A - Instantaneous firing rates of the neurons in the model during a seizure-like theta episode. Top row - LFP of a seizure-like theta episode simulated by the model with spr=0.6, scl=0.6, $E_K = -80mV$ and τ_{Cl}=1 second under wakefulness settings. Bottom four rows - Instantaneous firing rates of the excitatory (orange) and inhibitory (blue) neurons in the EC, DG, CA3 and CA1 regions of the model, in Hz. B - Instantaneous firing rates of the excitatory neurons in the model during one peak of a seizure-like theta episode, indicated with a black arrow on panel A.